Spectral Analysis Using Regularized Non-Negative Least-Squares Estimation

P. Chiao, J.A. Fessler, K.R. Zasadny, and R.L. Wahl
University of Michigan, Ann Arbor, MI

Abstract

The implementation of spectral analysis techniques involves solving a highly underdetermined linear system equation and is prone to the effect of measurement noise. We propose to use a regularized non-negative least-square estimator to stabilize the implementation of the technique. We introduce a penalty term in our formulation of the objective function to discourage disparities in tracer kinetics between neighboring pixels and use an iterative method to impose positivity constraints. We show results from analysis of FDG thorax images of patients suspected to have cancers and summarize our findings.

I. INTRODUCTION

Spectral analysis is a flexible non-parametric technique for characterizing the kinetic behavior of radiotracers. It has been known that for all biological systems, linear or nonlinear, if the system is injected by a tracer in a steady state, the distribution of the tracer follows the kinetics of a linear compartmental system, which has sums of exponential solutions [1]. Tobler [2] and Cunningham [3] wisely chose a set of exponential functions, convolved with the plasma input function, as basis functions. With such formulations, the time activity curve of a region or a pixel can be written as a linear combination of the basis functions with corresponding coefficients. The original implementation of the technique used a non-negative simplex method or non-negative least-squares to compute the coefficient of each basis function [2, 3]. Since this technique does not require a predefined compartmental structure and it can be used to characterize tracer kinetics in various tissue types or even mixtures of different tissue types, it provides a unique tool for image analysis of complex functional structures where image pixels may contain inhomogeneous tissue types. However, the implementation of the technique involves solving a highly underdetermined linear system equation and is prone to the effect of measurement noise.

We propose to use a regularized non-negative least-squares estimator (RNNLSE) to stabilize the implementation of the technique. We introduce a penalty term in our formulation of the objective function to discourage disparities in tracer kinetics between neighboring pixels. Since the number of parameters (the product of the number of pixels and the number of spectral coefficients for each pixel) is too large, the implementation of the estimator has to rely on iterative algorithms. We choose to use coordinate decent algorithms because it can naturally incorporate positivity constraints. To minimize a potential problem of loss of resolution due to spatial smoothing as a result of regularization, we also implement and compare edge-preserving penalty functions with quadratic penalty functions.

We hypothesize that RNNLSE can provide better spectral images for visual interpretation. To test our hypothesis, we compared RNNLSE with non-negative least-squares estimators (NNLSE) by analyzing images of patients who were suspected to have lung cancers and breast cancers and underwent PET FDG imaging. We chose to analyze FDG images in this preliminary investigation because the kinetic components of FDG are well-understood and FDG compartmental parameters can be easily related to spectral coefficients (making the interpretation of spectral images plausible).

In Section I, we review some properties of spectral analysis and give our formulation. Section II describes some implementation issues including criteria, penalty functions, and algorithms. Section III reviews the FDG compartmental model. Data analysis experiments are described in Section IV. Results are shown in Section V and discussion and future work in Section VI.

II. SPECTRAL ANALYSIS

We write the time activity of the j-th pixel $y_j(t)$ as a linear combination of a set of basis functions each of which has a coefficient x_{ij}

$$y_j(t) = \sum_{i=1}^{N} a_i(t) x_{ij} \tag{1}$$

where N (typical values of which is 100) is the number of basis functions and the i-th basis function $a_i(t)$ is related to the plasma time activity $B(t)$ and an exponential function $e^{-\beta_i t}$ as follows

$$a_i(t) = \int_0^t e^{-\beta_i (t-\tau)} B(\tau) d\tau.$$

The values of β_i are predetermined in order to cover an appropriate spectral range. Therefore, the only unknowns in (1) are the coefficients x_{ij}. We concatenate all the measured time activities (typical number of which is 20) of every pixel in a long vector Y, collect all corresponding terms $a_i(t)$ in a matrix A, concatenate all the x_{ij} in a vector X, and rewrite (1) as

$$Y = AX. \tag{2}$$

0-7803-3180-X/96$5.00©1996

Since the typical number of the basis functions is 5 times greater than that of measured time activities, (2) is a under-determined linear system and the solution of it is prone to the effect of measurement noise.

II. Implementation Issues

A. Criteria

The original implementation of spectral analysis used NNLSE, which is based on least-square criteria and constrained optimization techniques, and can be summarized as follows

$$\Phi(X) = (AX - Y)^T (AX - Y) \tag{3}$$

$$\hat{X} = \arg\min_X \Phi(X), \quad X \geq 0$$

where the solution $\hat{X}$ is constrained to be non-negative. Notice that this implementation does not have any spatial constraints. It allows neighboring pixels to have vastly different spectral coefficients and ,therefore, can potentially give noisy spectral images. To minimize this potential problem, we propose to incorporate a penalty in (3) to discourage disparities in the values of spectral coefficients between neighboring pixels as follows

$$\Phi(X) = (AX - Y)^T (AX - Y) + \alpha \sum_{i=1}^{N} P_i(X). \tag{4}$$

where $P_i(X)$ is spatially applied to the i-th spectral coefficients.

B. Penalty functions

The penalty terms in (4) have the following form

$$P_i(X) = \sum_j \sum_k w_{jk} \theta(x_{ij} - x_{ik}) \tag{5}$$

where w_{jk} equals to 1 for horizontal and vertical neighboring pixels and is zero otherwise. We choose to use a quadratic penalty

$$\theta(s) = s^2 \tag{6}$$

and an edge-preserving penalty [4]

$$\theta(s) = \delta^2 \left(|s/\delta| - \ln(1 + |s/\delta|) \right). \tag{7}$$

where δ can be adjusted to achieve the desired edge-preserving effect. Figure 1 shows some properties of (7).

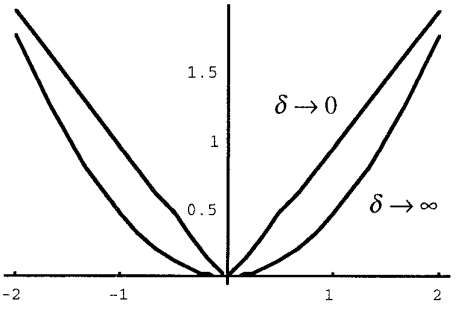

Fig. 1. Plots of normalized edge preserving functions. The function becomes quadratic when $\delta \to \infty$ and it approaches an absolute function when $\delta \to 0$.

C. Algorithms

Since the dimension of A in (2) is too large, the implementation of RNNLSE has to rely on iterative algorithms. We choose to use coordinate decent algorithms because it can naturally incorporate positivity constraints. Thus, in each iteration n we sequentially update every x_{ij} using the 1D Newton's method by fixing other parameters at their current values as follows

$$x_{ij}^{n+1} = x_{ij}^n - \frac{\frac{\partial}{\partial x_{ij}} \Phi(X)\Big|_{x_{ij}=x_{ij}^n}}{\frac{\partial^2}{\partial x_{ij}^2} \Phi(X)\Big|_{x_{ij}=x_{ij}^n}} \tag{8}$$

$$x_{ij}^{n+1} = \max\left\{ x_{ij}^{n+1}, 0 \right\}.$$

When quadratic penalty functions are used, (8) has one step solution. However, when edge-preserving is used, few iterations of (8) are required to achieve sufficient decreases in the objective function value. Thus, in each step of (8), the minimum of the objective function in the subspace spent by the parameter x_{ij} will either be reached or approached further.

III. FDG Compartmental Model

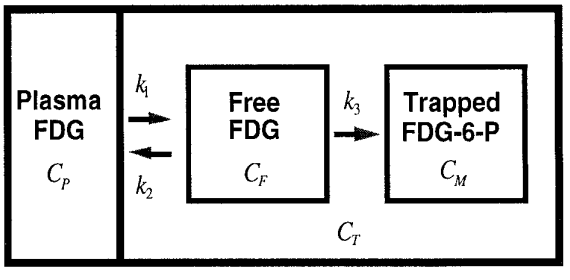

Fig. 2. Schematic diagram of FDG compartmental model.

The compartmental model of FDG is summarized in Fig. 2. k_1 and k_2 characterize the rates of exchange of

FDG between the plasma and tissue compartments. FDG as an analog of glucose can be phosphorylated to FDG-6-P and trapped in the cellular space. This process is described by k_3. The total tissue time activity $C_T(t)$ is the sum of the free FDG time activity $C_F(t)$ and trapped FDG-6-P time activity $C_M(t)$. By solving the underlying linear differential equations, $C_T(t)$ can be written as

$$C_T(t) = \left[\frac{k_1 k_3}{k_2 + k_3}\right]\int_0^t C_P(\tau)d\tau + \left[\frac{k_1 k_2}{k_2 + k_3}\right]\int_0^t C_P(\tau)e^{-(k_2+k_3)(t-\tau)}d\tau. \quad (9)$$

It can be shown [5] that the glucose metabolism rate is proportional to $k_1 k_3/(k_2 + k_3)$ and is therefore proportional to the first term in (9), which in turn corresponds to the first spectral component where the exponent $\beta_1 = 0$. Knowing this, we consider the image of the first spectral coefficients as a map of glucose metabolism rates.

IV. Experiments

PET FDG thorax images of 3 patients suspected to have lung cancers (n=2) and breast cancers (n=1) were analyzed using both RNNLSE and NNLSE. Twenty-five time frames were acquired over 60 minutes: 12 x 10 sec, 3 x 20 sec, 2 x 60 sec, 5 x 300 sec, and 3 x 600 sec. Eighty basis functions with exponent values ranging from 0 to 3 /min were used and were spaced logarithmically. Input functions were determined from a region drawn on either left atrium or ascending aorta. Results provided by NNLSE were used to initialize RNNLSE, which was carried out for 100 iterations. δ in edge-preserving penalty functions was set to 0.01. To save computation, images were clipped to smaller size.

V. Results

RNNLSE showed significant improvement over NNLSE in the analysis of images from one patient suspected to have lung cancers (see Fig. 3(a)-(d)). While the image of the first spectral coefficients (Fig. 3(c)) provided by RNNLSE with the quadratic penalty function (RNNLSE-Q) resembles late FDG images (Fig. 3(a)) in the shape of the hot spot region of interest (ROI) and has superior ROI-to-tissue contrast, the image provided by NNLSE (Fig. 3(b)) is noisy and in some cases even fails to show the complete shape of the hot spot ROI. RNNLSE with edge-preserving penalty functions (RNNLSE-E) does not show discernible sharpening effects. However, RNNLSE-E provides a significantly better fit to the dynamic image data than RNNLSE-Q does and almost resemble the fit provided by RNNLSE (see Fig. 4). The patient underwent bronchoscopy and was confirmed to have inflammatory tissues in the region delineated by the hot spot.

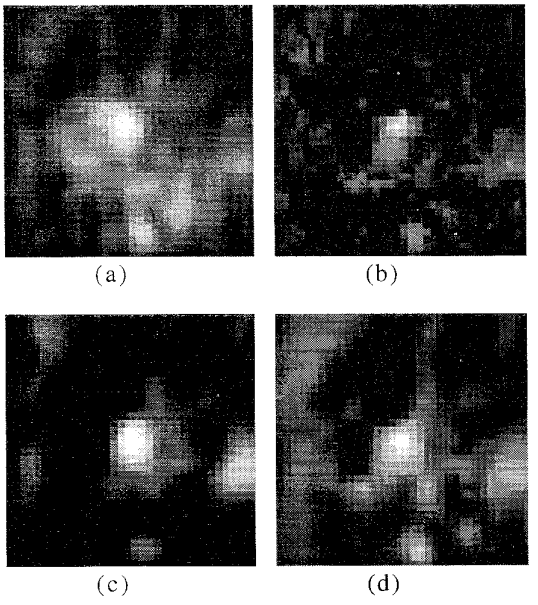

Fig. 3. Images of the first spectral coefficients from a patient suspected to have lung cancers and was confirmed only to have inflammatory tissues. (a) Late FDG image. (b) Using NNLSE. (c) Using RNNLSE-Q. (d) Using RNNLSE-E.

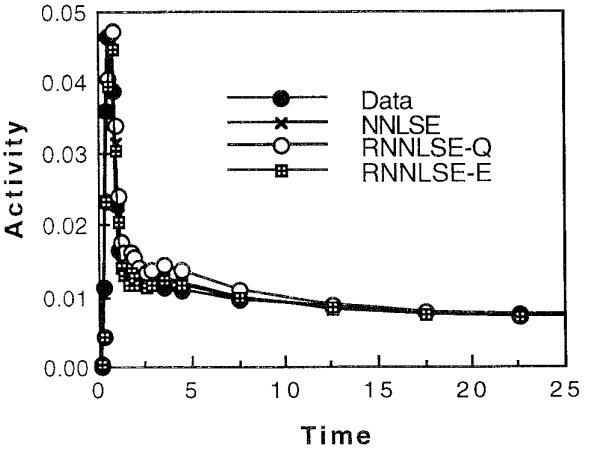

Fig. 4. Each curve is an average of all the pixel been analyzed. While RNNLSE-E and NNLSE both provide a close fit to the data, RNNLSE-Q does not.

All estimators provided improved tumor-to-tissue contrast in the analysis of images from a patient confirmed to have malignant lung tumors (see Fig. 5(a)-(d)). The image provided by NNLSE shows the sharpest tumor outline (Fig. 5(b)) at expense of more noise. Both RNNLSE-E and RNNLSE-Q provide cleaner images. RNNLSE-E only provides marginal improvement over RNNLSE-Q in preserving the tumor outline. Analysis of the

patient suspected to have breast cancers showed similar results and images are not shown here.

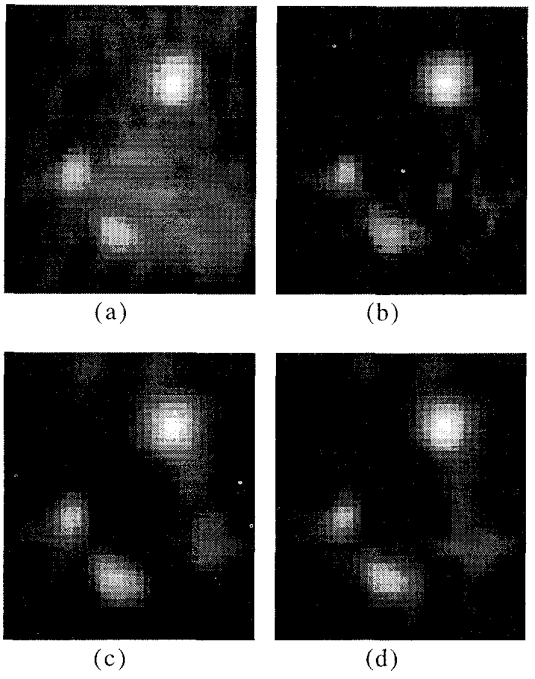

Fig. 5. Images of the first spectral coefficients from a patient confirmed to have malignant lung tumors. (a) Late FDG image. (b) Using NNLSE. (c) Using RNNLSE-Q. (d) Using RNNLSE-E.

VI. Discussion and Future Work

Results of our qualitative evaluation of RNNLSE in comparison with NNLSE are mixed. For all patients (n=2) confirmed to have malignant tumors, both RNNLSE-Q and RNNLSE-E provided cleaner images than those provided by NNLSE. However, NNLSE provided the sharpest tumor outlines. For the patient confirmed to have inflammatory tissues, RNNLSE bettered NNLSE significantly in every visual aspect. It is well known that inflammotory tissues can have intensive FDG uptakes and may cause difficulties in detecting tumors solely by visual interpretation of FDG images. In addition, differences in FDG kinetics between inflammotory tissues and tumors are not well understood. Therefore, we are unable to comment on the inferior performance of NNLSE in the analysis of images from the patient having inflammotory tissues (compare Fig. 3(b) with Fig. 5(b)) and its significance to our qualitative comparison between NNLSE and RNNLSE.

Future work includes the following. (1) Investigate the selection of penalty functions and understand their effects on spectral coefficients. (2) Investigate strategies for selecting the optimal δ for RNNLSE-E. (2) Investigate the significance of the number of non-zero and zero spectral coefficients. For example, we have observed significant lower numbers of zero coefficients using RNNLSE (in one case 10 times lower). (3) Design optimal spacing for the exponents. (4) Design optimal data acquisition schedules and shapes of input functions. (5) Quantitatively study the property of RNNLSE and NNLSE. (6) Develop display methods to facilitate the interpretation of spectral coefficients.

References

[1] J. A. Jacquez, *Compartmental Analysis in Biology and Medicine*, 2nd. ed. Ann Arbor: The University of Michigan Press, 1988.

[2] H. J. Tobler and G. Engel, "Affinity spectra: a novel way for the evaluation of equilibrium binding experiments" *Naunyn Schmiedebergs Arch Pharmacol*, vol. 322, pp. 183-92, 1983.

[3] V. J. Cunningham and T. Jones, "Spectral analysis of dynamic PET studies" *J Cereb Blood Flow Metab*, vol. 13, pp. 15-23, 1993.

[4] K. Lange, Convergence of EM image reconstruction algorithms with Gibbs smoothing. *IEEE Tr. Med. Im.*, 9(4):439-446, Dec. 1990.

[5] M. E. Phelps, J. C. Mazziotta and H. R. Schelbert, *Positron Emission Tomography and Autoradiography Principles and Applications for the Brain and Heart*. New York: Raven Press, 1986.